Santamarina, C. & Cascante, G. (1998). *Géotechnique* **48**, No. 1, 129–136

TECHNICAL NOTE

Effect of surface roughness on wave propagation parameters

C. SANTAMARINA* and G. CASCANTE†

KEYWORDS: dynamics; laboratory tests; microscopy; stiffness; vibration; waves and wave loading.

INTRODUCTION

The behaviour of particulate materials is directly affected by their fabric, the imposed state of stress and the inherent characteristics of particles, for example mineralogy, size, material strength and stiffness, angularity and surface characteristics. In general, the characteristics of individual particles have limited effect on the large-strain macrobehaviour of soils. However, experimental results obtained by the authors and other researchers show that the properties of particles do affect small-strain parameters.

The purpose of this note is to review the effect of surface characteristics on soil phenomena, and to report experimental results on the role of surface roughness on wave propagation parameters.

LITERATURE REVIEW

Small compared with large strain

Slade & Walton (1993) derived relations based on Mindlin contact and found that the longitudinal wave velocity in a random packing of spheres is a non-linear function of the interparticle friction coefficient. However, surface conditions affect the behaviour of granular materials in complex ways, sometimes causing opposite trends at different strain levels. In general, the more pronounced asperities are, the lower the small-strain stiffness of the medium ($\gamma < \approx 10^{-4}$), although surface roughness increases peak and residual strengths, even when particle rolling occurs.

Effective stress and shear strength

Skempton (1960) reassessed Terzaghi's effective stress principle and suggested two alternative interpretations, one related to compressibility and the other to strength. Skempton's definition of effective stress σ' for shear strength depends on the intrinsic angle of interparticle friction ϕ_u and on the angle of shear resistance ϕ:

$$\sigma' = \sigma - \left(1 - a\frac{\tan\phi_u}{\tan\phi}\right)u \tag{1}$$

where σ is the total stress, u is the pore pressure and a is the contact area between particles per unit gross area. For volume change, the effective stress σ' relates to the compressibility C of the particulate material (which is affected by surface roughness and contact response) and the compressibility C_s of the material comprising the particles:

$$\sigma' = \sigma - \left(1 - \frac{C_s}{C}\right)u \tag{2}$$

Different rearrangement mechanisms affect the residual angle of shear resistance rolling shear, transitional shear and sliding shear (Mitchell, 1993). Experimental evidence shows that the angle of residual shear resistance in sands decreases with clay content, while the difference between the peak and the residual angles of shear resistance increases. Considering that clay particles 'coat' sand particles, smoothing their surface, these observations suggest that surface roughness alters the particle rearrangement mechanism at high shear deformations.

Bishop (1954) derived an approximate expression for the constant-volume angle of shear resistance ϕ_{cv} for triaxial compression, in terms of the interparticle friction angle ϕ_u:

$$\sin\phi_{cv} = \frac{15\tan\phi_u}{10 + 3\tan\phi_u} \tag{3}$$

Relations between ϕ_{max} and ϕ_u have been proposed for regular packings of monosized spheres and for isotropic random packings (Horne, 1965); for example,

$$\tan^2\left(\frac{\pi}{4} + \frac{\phi_{max}}{2}\right) = 2\tan\left(\frac{\pi}{4} + \phi_u\right) \tag{4}$$

Manuscript received 17 June 1996; revised manuscript accepted 8 October 1996.
Discussion on this technical note closes 1 May 1998; for further details see p. ii.
* Georgia Institute of Technology, Atlanta.
† University of Waterloo.

Finally, ϕ_{max} and ϕ_{cv} are related through the dilatancy ψ of the material (e.g. Bolton, 1986):

$$\phi_{max} = \phi_{cv} + 0{\cdot}8\psi_{max} \quad (5)$$

In contrast to these analytical predictions, experimental results by Skinner (1969) showed no effect of the intrinsic angle of interparticle friction ϕ_u on ϕ_{cv}. He concluded that particle rolling explained the differences (see Bishop, 1971; Rowe, 1971). He modified the friction coefficient μ by wetting, rather than by changing surface roughness.

Water, surface layers and ϕ_u

Water has no effect on the coefficient of friction μ on chemically clean quartz surfaces. However, μ increases in the presence of water when surfaces are not clean, owing to the disruption of adsorbed films that serve as lubricants for dry surfaces. This effect is observed when the surface roughness varies between 50 and 1500 nm (Feda, 1982). The effect of water as an anti-lubricant diminishes for rougher surfaces (Procter & Barton, 1974). Other studies have also shown that different chemical fluids and material molecular structures affect ϕ_u (Rowe, 1971; Mitchell, 1993). In general, adsorbed layers reduce μ in mineral granular materials because they reduce the effective area of solid contact between particles (the adhesion theory of friction, Bowden & Tabor, 1982).

Skinner (1969) found an increase in the coefficient of friction μ by a factor of ten when glass spheres were water-flooded in comparison with when they were dry ($\mu = 0{\cdot}08$ to $\mu = 0{\cdot}79$; the text indicates potential changes between 3·5 and 30 times); no details were given about surface conditions. Ishibashi *et al.* (1994) found an increase in μ by almost a factor of two when glass spheres were flooded ($\mu = 0{\cdot}162$ to $\mu = 0{\cdot}277$).

Contact force and ϕ_u

Feda (1982) reported that the friction coefficient μ of dry glass spheres differs from that in flooded conditions when the normal contact load f_n is less than 10 N. Rowe (1971) argued that the interparticle friction angle ϕ_u should be inversely proportional to the cube root of the load f_n in a Hertzian contact, since the contact area is proportional to the contact load raised to the power $\frac{2}{3}$. Thus, he justified a decrease of ϕ_u with an increase in particle size. (Note that for the same average coordination number, the larger the particle size, the higher the force at contacts $f_n \approx 4\sigma R^2$.) Published data both support and contradict this prediction. Procter & Barton (1974) found no apparent variation in ϕ_u for normal forces in the range $0{\cdot}1 < f_n < 0{\cdot}6$ N whereas Skinner (1969) observed a significant increase in ϕ_u with normal force in the range $0{\cdot}06 < f_n < 1{\cdot}1$ N, for glass spheres, steel spheres and lead shot (diameters 1 mm and 3 mm).

Numerical micromechanics

Micromechanical simulations of random arrays of monosized spheres by Cambou (1993) predicted the angle of internal shear strength ϕ to be strongly dependent on the interparticle friction angle ϕ_u when ϕ_u is low, with ϕ remaining constant when ϕ_u exceeds 20°–30°. Thornton & Sun (1993) found that ϕ and stress-induced anisotropy increase with ϕ_u in three-dimensional simulations of axisymmetric compression loading of monosized spheres.

Absorbed layers and small-strain parameters

The presence of absorbed layers determines the nature of the loss mechanism in small-strain wave propagation and has some effect on the exponent of the velocity–stress power relationship, especially at low contact forces. Duffy & Mindlin (1957) cleaned steel spheres in successive baths of carbon tetrachloride, toluol and acetone to avoid the effect of absorbed layers. In addition, capillary forces produced by fluid menisci in partially saturated particulate media affect the effective stress, the shear strength and small-strain parameters such as wave velocity (Biarez *et al.*, 1993; Aitchison & Donald, 1956; Chang *et al.*, 1990, 1991).

Summary

Studies on the effect of surface characteristics and interparticle friction on small- and large-strain phenomena are limited and results are often contradictory. Such contradictions may reflect the complex effects of wetting and contact forces on ϕ_u, and the effects of dilation and particle rotation.

RELATIONS FOR VELOCITY AND ATTENUATION

Empirical expressions for the small-strain shear modulus G_{max} in soils under isotropic loading σ_0 are of the following form:

$$G_{max} = Af(e)\sigma_0^{2b} \quad (6)$$

Given that $V_s = \sqrt{(G/\rho)}$, then

$$V_s = a\sigma_0^b \quad (7)$$

where A, a and b are constants, and $f(e)$ is a function of void ratio (e.g. Hardin & Drnevich, 1972; Stokoe *et al.*, 1985; Saxena *et al.*, 1988). This empirical equation is remarkably similar to micromechanics-based equations for random packings of spheres (Chang *et al.*, 1991; Santamarina

& Cascante, 1997). The exponent b reflects the nature of the contact and fabric changes. At *constant fabric*, $b = \frac{1}{6}$ for Hertzian contact and $b = \frac{1}{4}$ for conical contact.

Expressions for attenuation under different contact laws are scarce. Considering frictional attenuation and regular packings (FCC and SC), the damping at small strain D decreases with confinement σ_0 as

$$D = C\sigma_0^{\kappa} \tag{8}$$

where C is a constant. The exponent for Mindlin contacts is $\kappa = -\frac{2}{3}$ (Duffy & Mindlin, 1957; Petrakis & Dobry, 1987). The attenuation α of a plane wave can be calculated from D using

$$\alpha = 2\pi\frac{D}{\lambda} \tag{9}$$

where λ is the wavelength. The variation of damping with confinement and strain can be modelled with hyperbolic models (Ishihara, 1986). Experimental evidence shows that the contribution of frictional loss diminishes at small strains $\gamma < 10^{-5}$, and other loss mechanisms are involved. Hyperbolic models must be modified to account for these losses at small strains (Santamarina & Cascante, 1996).

SPECIMEN PREPARATION

The effect of surface roughness on wave propagation parameters was studied experimentally with high-tolerance steel spheres, diameter $d = 3{\cdot}18 \pm 0{\cdot}00254$ mm, specific gravity $G_s = 7{\cdot}81$. The approximate number of particles in each sample was 19 000. Surface roughness was altered by successive cleaning and corrosion stages imposed on the same batch of steel spheres. 'As received' ball bearings were first washed with acetone and dried with a lint-free cloth.

The first specimen, 'mild rust', was obtained by washing steel spheres with detergent (Alconox). Afterwards, the spheres were cleaned with acetone, dried with a lint-free cloth and tested 24 h later. Rust pitting could be seen by eye, even though the spheres remained shiny.

The second specimen, 'rusted', was obtained by immersing the spheres in Alconox detergent. The spheres were then washed with acetone and submerged for 24 h in Okaite (a hydrochloric acid solution). Finally, they were rinsed in water and left in air overnight for further rusting. The spheres lost all lustre.

Scanning electron microscope (SEM) pictures of the two specimens tested are presented in Figs 1 and 2. Magnifications of 1000 and 10 000 times cover the scale of expected contact areas. Assuming a simple cubic array and the elastic properties of steel ($G = 82{\cdot}74$ MPa, $\nu = 0{\cdot}21$), Hertz's theory predicts the radii of contact to be 14 μm and 25 μm for 50 kPa and 250 kPa confinement respectively. On the other hand, if a uniform stress distribution is assumed at a yielding contact ($\sigma = \sigma_\gamma$), the computed radii of contact are 26 μm and 57 μm, for the same confining loads. SEM pictures show that the increase in surface roughness has a noticeable effect on the size of the asperities at the scale of the contact area. It is informative to compare these photographs with each other, and with the theoretical assumptions made in contact models, for example smooth spherical surface in Hertzian contact and conical surface in cone-to-plane contact.

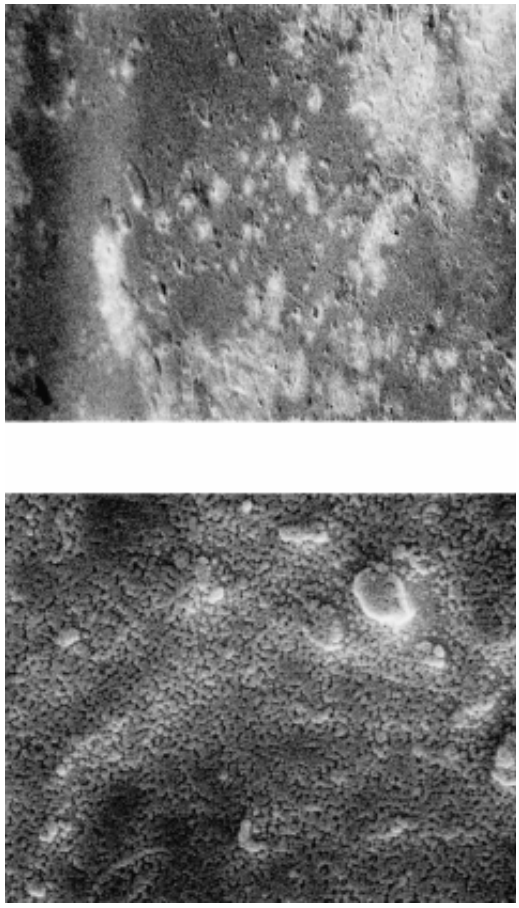

Fig. 1. Specimen 1 (mild rust): SEM photographs of surface features; width of area shown (a) 100 μm; (b) 10 μm

Cylindrical specimens were prepared within a resonant column device with load-control deviatoric loading capability (Cascante & Santamarina, 1996). A standard split mould and latex membrane were used. Gypsum paste was added to the end

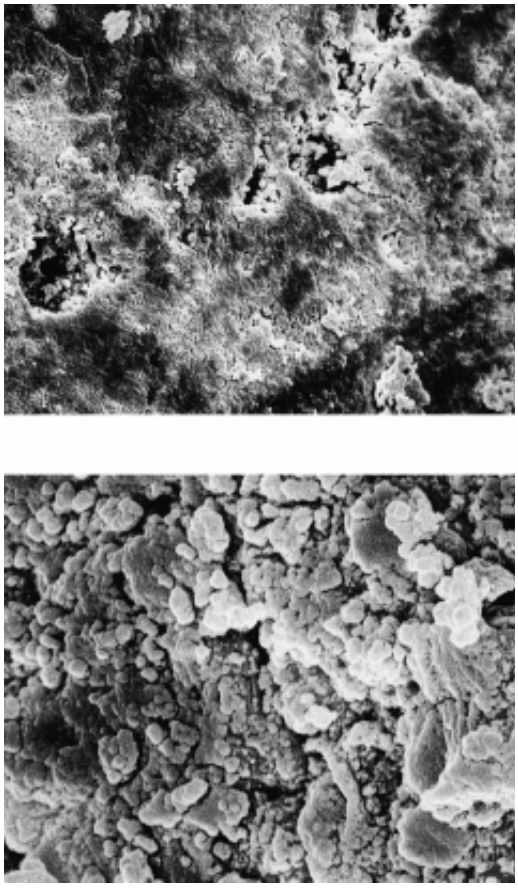

Fig. 2. Specimen 2 (rusted): SEM photographs of surface features; width of area shown (a) 100 μm; (b) 10 μm

plates to enhance coupling. Ball bearings were slowly rained through a funnel and densified by light tamping. Gypsum penetrated the specimen by approximately 10 mm at the top and 6 mm at the bottom and after setting, a vacuum was applied to remove the split mould (−94 kPa). The sample was kept under constant confinement of $\sigma_0 = 50$ kPa for approximately 2 h until the gypsum hardened. Afterwards, isotropic confinement was increased in stages until the maximum stress of $\sigma_0 = 250$ kPa was reached. This maximum load was selected to avoid significant plastic deformation at contacts. Resonant column testing was performed at each load level.

Similar specimens were tested under axial compression loading within the same device, to determine the large-strain load–deformation response ($\sigma_0 = 200$ kPa; no gypsum coupling was used in these tests).

The initial void ratio for all samples was $e \approx 0{\cdot}60$, which is close to the general value for a random assembly of smooth monosized spheres (Scott *et al.*, 1964). The main characteristics of specimens 1 and 2 are summarized in Table 1.

EXPERIMENTAL RESULTS

Large-strain load–deformation data are plotted in Fig. 3. A third specimen is included, made with the steel spheres as received. The angle of shear resistance ϕ increases with surface roughness (Fig. 3(a), equation (4)); however, the small-strain stiffness decreases (Fig. 3(b)).

Resonant column test results for specimen 1 during isotropic loading are presented in Fig. 4. The $\sigma_0 - \varepsilon_z$ curve shows a maximum axial strain $\varepsilon_{max} = 250$ μs and a residual axial strain $\varepsilon_r =$

Table 1. Summary of test results

	As received	Mild rust (specimen 1)	Rusted (specimen 2)
Void ratio	0·60	0·61	0·62
Friction angle ϕ (no gypsum)	19·6	19·6	22·2
Maximum axial strain: %	—	0·025	0·041
Residual strain: %	—	0·005	0·018
Exponent b, load (unload)	—	0·14 (0·15)	0·16 (0·22)
Constant $\log(a)$, load (unload)	—	2·17 (2·15)	2·01 (1·89)
Exponent κ, load (unload)	—	−0·41 (−0·45)	≈0 (≈0)
$\log(\gamma_{max})$ range	—	−5·8 to −5·9	−5·4 to −5·7
Velocity range: m/s	—	230 to 315	150 to 250
Damping range: ($\times 10^{-3}$)	—	45 to 17	18 to 14

* Elastic spherical contact (Hertz) $b = \frac{1}{6}$
Elastic cone–plane contact $b = \frac{1}{4}$
Plastic spherical contact $b = \frac{1}{4}$
Hysteretic loss (Mindlin) $\kappa = -\frac{2}{3}$

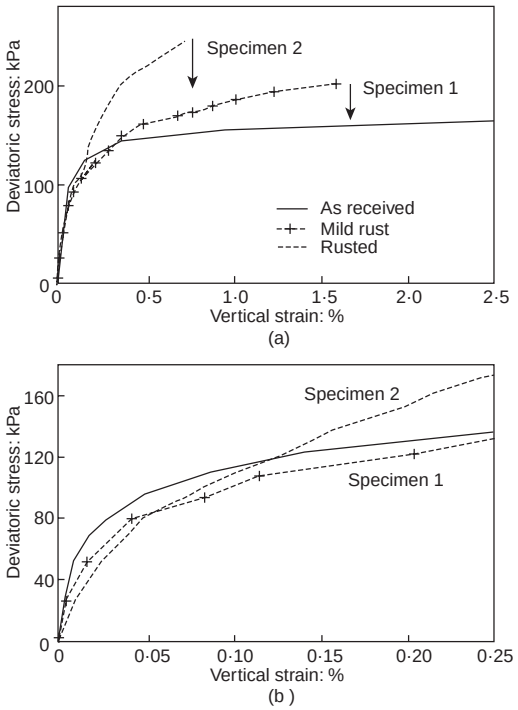

Fig. 3. Large-strain deviatoric loading ($\sigma_2 = \sigma_3$)

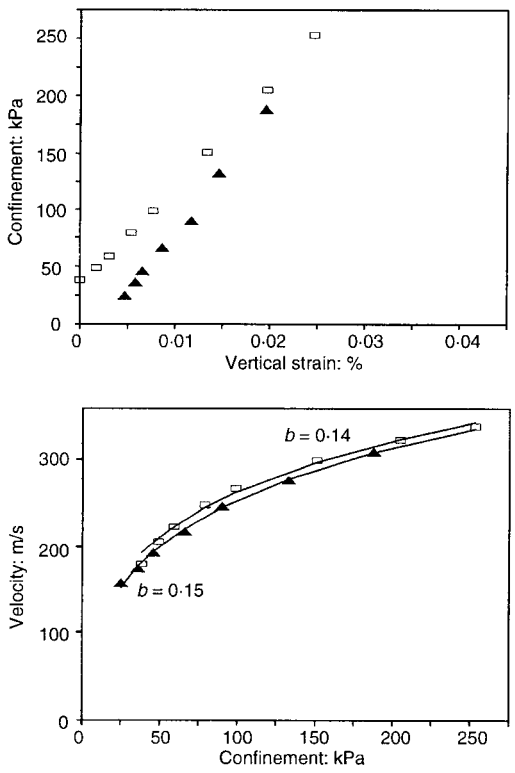

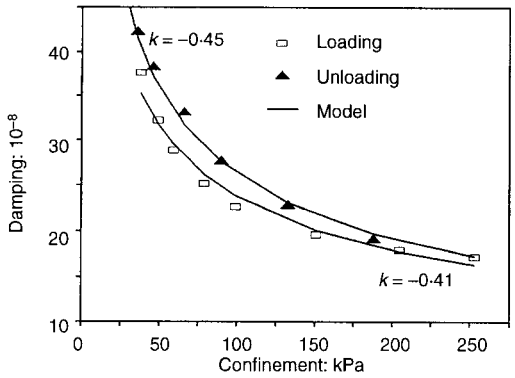

Fig. 4. Specimen 1 (mild rust) under isotropic confinement: variation of low-strain velocity and damping with confinement

50 μs (Fig. 4(a)). The velocity–stress exponent $b = 0{\cdot}14-0{\cdot}15$ (loading–unloading) approaches the theoretical value $b = \frac{1}{6}$ (Fig. 4(b)). The damping coefficient D showed a similar trend during loading and unloading with $\kappa = -0{\cdot}41$ to $-0{\cdot}45$ (equation (8)).

The isotropic $\sigma_0-\varepsilon_z$ response during the loading of specimen 2, made from spheres with a rougher surface, is clearly different from that of specimen 1 (Fig. 5(a)). At the end of loading, this specimen was left overnight under $\sigma_0 = 250$ kPa, increasing the permanent deformation by 40 μs ($\varepsilon_{max} = 410$ μs, $\varepsilon_r = 180$ μs). The shear wave velocity was lower for specimen 2, and the velocity–stress exponent is $b = 0{\cdot}22$ during loading and $b = 0{\cdot}16$ during unloading (Fig. 5(b)). Damping showed low sensitivity to confinement, with $\kappa \approx 0$ (Fig. 5(c)). The dependence of wave velocity and damping on strain level is shown in Fig. 6 for an isotropic confinement $\sigma_0 = 254$ kPa.

DISCUSSION

Deviatoric loading

The initial tangential stiffness decreases with the increase of rust because of the softening effect of asperities: spikes and protuberances have low longitudinal and flexural stiffness and restrict the number of asperities touching per contact. Therefore, while the total area of contact may be the same in both specimens, the deformation of asperities leads to a reduction in global stiffness.

The angle of internal shear strength ϕ increases with surface roughness. There are two main components in ϕ: dilatancy and interparticle friction. The lower the void ratio, the higher the angle of dilatancy. At the same time, as the void ratio

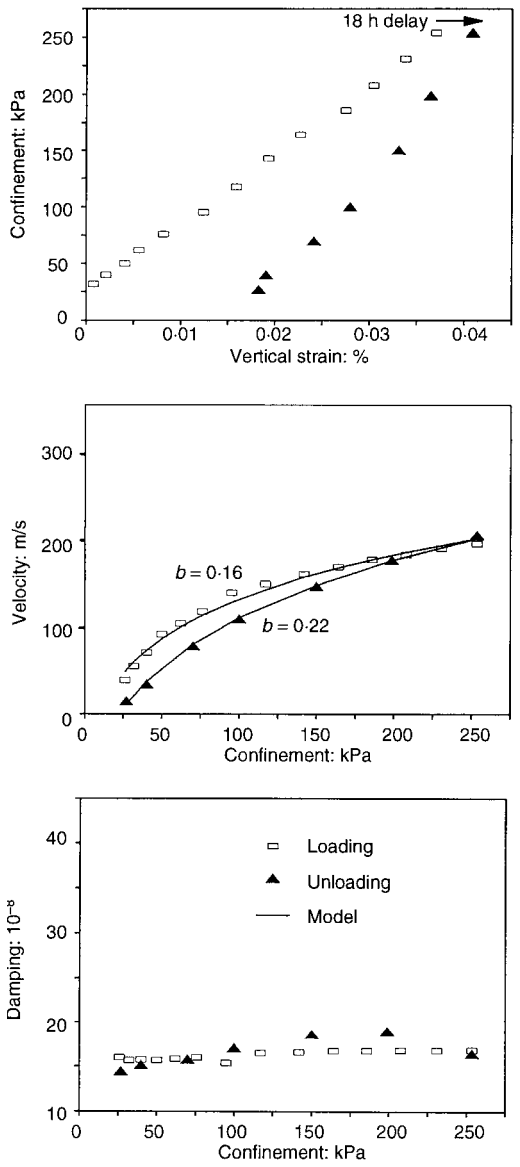

Fig. 5. Specimen 2 (rusted) under isotropic confinement: variation of low-strain velocity and damping with confinement

decreases, the higher coordination between particles increases the probability of particle rotational frustration, which must be overcome by slippage at contacts. Slippage is controlled by surface roughness, that is, ϕ_u. Therefore, the effect of surface roughness on the peak angle of internal shear strength should be more pronounced for dense materials.

Small-strain velocity

The decrease in velocity with the increase in surface roughness is in agreement with the observed behaviour in the stress–strain plot at low axial strains. As corrosion advances, the velocity–stress exponent b increases, reflecting not only the changes from spherical to conical contact geometry but also the higher susceptibility of rusted spheres to fabric changes with changes in confinement. During loading, the exponent is higher at low stress; it is possible to conceive situations where early loading will break asperities, and thereafter the stiffness of the contact will be controlled by the global geometry of the contact.

Small-strain damping

The decrease in damping with increased roughness may reflect the ability of asperities to penetrate adsorbed layers more easily than curved surfaces (Feda, 1982). Then, the probability of slippage decreases with the improved adhesion and interlocking between surfaces.

As surface roughness increased from specimen 1 to specimen 2, damping became stress-independent, as in an ideal cemented continuum (Fig. 5(c)). This demonstrates a significant change in the role of friction in energy dissipation when the contact changes from smooth Hertzian to rough-conical (changes in chemical composition affect adhesion). Asperities on a rusted surface may also alter the pressure distribution at contacts with non-zero values at the border of the contact area (compared with the parabolic distribution for a smooth surface). The annulus of slippage in a Mindlin contact is then reduced, decreasing frictional losses. When the strain level of the excitation in increased, asperity adhesion is overcome and friction prevails again, generating the typical strain-dependent losses for particulate media (Fig. 6).

CONCLUSIONS

Surface roughness decreases contact stiffness and increases the interparticle friction. The effect of these parameters on the macrobehaviour of a particulate medium must be analysed, distinguishing between small-strain, constant fabric excitation and large-strain phenomena.

As surface roughness increases, shear wave velocity decreases ($\gamma \approx 10^{-6}$), reflecting the lower stiffness of asperities. This is also noticed in the tangential modulus in triaxial tests ($\varepsilon \approx 10^{-4}$). The velocity–stress exponent b increases with surface roughness.

Damping becomes stress-independent as surface roughness increases. This is a marked deviation from the standard friction loss model (Mindlin contact). The presence of rust asperities may

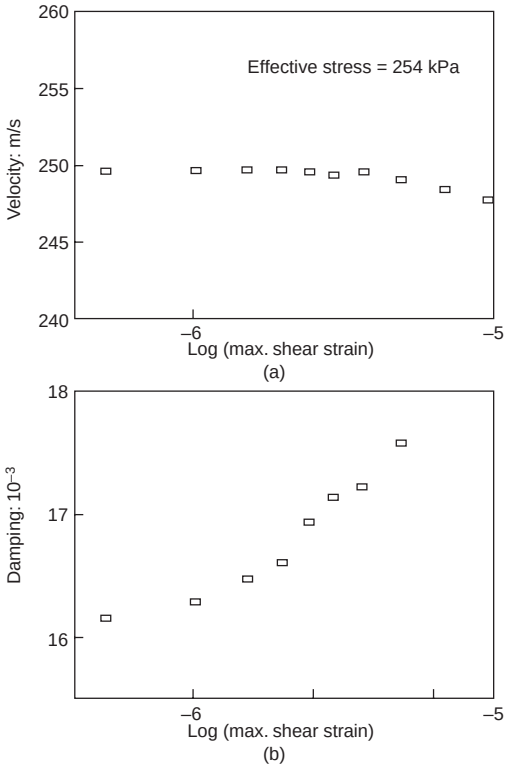

Fig. 6. Specimen 2 (rusted) at constant isotropic confinement: (σ_0 = 254 kPa): variation of velocity and damping with strain

affect adhesion and change the distribution of normal forces at the edge of contacts, diminishing the formation of the annulus of slippage. Nevertheless, the strain dependency of attenuation still follows the typical trend expected for hysteretic behaviour.

While small-strain stiffness decreases with surface roughness, large-strain stiffness and the angle of shear resistance increase with surface roughness. It is hypothesized that the contribution of surface roughness to large-strain parameters is more pronounced in dense materials where the probability of particle 'rotational frustration' increases.

ACKNOWLEDGEMENTS

This study was conducted by the authors during their affiliation with the University of Waterloo. Support was provided by the Natural Sciences and Engineering Research Council of Canada (NSERC) and the University of Waterloo ID-Program. The authors are indebted to Dr N. Yassir for thoughtful comments and suggestions.

REFERENCES

Aitchison, G. D. & Donald, I. B. (1956). Effective stress in unsaturated soils. *Proc. 2nd Australia–New Zealand Conf. on Soil Mechanics*, pp. 192–199.

Biarez, J., Fleureau, J. M. & Taibi, S. (1993). Constitutive model for unsaturated granular media. In *Powders and grains* (ed. C. Thornton), pp. 51–58. Rotterdam: Balkema.

Bishop, A. W. (1954). Correspondence on shear characteristics of a saturated silt, measured in triaxial compression. *Géotechnique* **4**, No. 1, 43–45.

Bishop, A. W. (1971). Shear strength parameters for undisturbed and remoulded soil specimens. In *Stress–strain behaviour of soils* (ed. R. G. H. Parry), pp. 3–58. Cambridge.

Bolton, M. D. (1986). The strength and dilatancy of sands. *Géotechnique* **36**, No. 1, 65–78.

Bowden, F. P. & Tabor, D. (1982). *Friction—an introduction to tribology.* Florida: Krieger.

Cambou, B. (1993). From global to local variables in granular materials. In *Powders and grains* (ed. C. Thornton) pp. 73–86. Rotterdam: Balkema.

Cascante, G. & Santamarina, J. C. (1997). Low strain measurements with resonant-column apparatus. *Geotech. Testing J.* **20**, No. 1, 29–39.

Chang, T., Misra, A. & Sundaram, S. S. (1990). Micromechanical modeling of cemented sands under low amplitude oscillations. *Géotechnique* **40**, No. 2, 251–263.

Chang, C. S., Misra, A. & Sundaram, S. S. (1991). Properties of granular packings under low amplitude cyclic loading. *Soil Dyn. Earthq. Engng* **10**, No. 4, 201–211.

Duffy, J. & Mindlin, R. D. (1957). Stress–strain relations of a granular medium. *J. Appl. Mech.* **24**, No. 4, 585–593.

Feda, J. (1982). Mechanics of particulate materials—the principles. In *Developments in geotechnical engineering*, Vol. 30. New York: Elsevier-Academia.

Hardin, B. O. & Drnevich, V. P. (1972). Shear modulus and damping in soils: measurements and parameter effects. *J. Soil Mech. Fdns Engng, ASCE* **98**, 603–624.

Horne, M. R. (1965). The behavior of an assembly of rotund, rigid, cohesionless particles. Part I. *Proc. Royal Society of America* **286**, 62–78.

Ishibashi, I., Perry, C., III & Agarwal, T. K. (1994). Experimental determinations of contact friction for spherical glass particles. *Soils Fdns* **34**, No. 4, 79–84.

Ishihara, K. (1986). Evaluation of soil properties for use in earthquake response analysis. In *Geomechanical modeling in engineering practice* (eds R. Dungar and J. A. Studer). Rotterdam: Balkema.

Mitchell, J. K. (1993). *Fundamentals of soil behavior*, 2nd edn. New York: Wiley.

Petrakis, E. & Dobry, R. (1987). *Micromechanical modeling of granular soil at small strain by arrays of elastic spheres*. Report CE-87-02, Department of Civil Engineering, Rensselaer Polytechnic Institute, Troy, NY.

Procter, D. C. & Barton, R. R. (1974). Measurements of the angle of interparticle friction. *Géotechnique* **24**, No. 4, 581–604.

Rowe, P. W. (1971). Theoretical meaning and observed

values of deformation parameters for soils. In *Stress–strain behaviour of soils* (ed. R. G. H. Parry), pp. 143–194. Cambridge.

Santamarina, J. C. & Cascante, G. (1996). Stress anisotropy and wave propagation—a micromechanical view. *Can. Geotech. J.* **33**, No. 5, 770–782.

Saxena, S. K., Avramidis, A. S. & Reddy, K. R. (1988). Dynamic moduli and damping ratios for cemented sands at low strains. *Can. Geotech. J.* **25**, 353–368.

Scott, G. D., Charlesworth, A. M. & Mark, M. K. (1964). On the random packing of spheres. *J. Chem. Phys.* **40**, 611–612.

Skempton, A. W. (1960). Effective stress in soils, concrete and rocks. *Proc. Pore Pressure and Suction in Soils Conf.*, pp. 4–16. London: Butterworth.

Skinner, A. E. (1969). A note on the influence of interparticle friction on a shearing strength of a random assembly of spherical particles. *Géotechnique* **19**, No. 1, 150–157.

Slade, R. E. & Walton, K. (1993). Inter-granular friction and the mechanical and acoustic properties of granular media. In *Powders and grains* (ed. C. Thornton) pp. 93–98. Rotterdam: Balkema.

Stokoe, K. H., Lee, S. H. & Knox, D. P. (1985). Shear moduli measurements under true triaxial stresses. *Proc. Advances in the Art of Testing Soils Under Cyclic Conditions*, pp. 166–185. Detroit: ASCE.

Thornton, C. & Sun, G. (1993). Axisymmetric compression of 3D polydisperse systems of spheres. In *Powders and grains* (ed. C. Thornton) pp. 129–134. Rotterdam: Balkema.